

# Peer-Reviewed Technical Communication

## Frequency-Domain Decision Feedback Equalization for Single-Carrier Transmissions in Fast Time-Varying Underwater Acoustic Channels

Xingbin Tu, Xiaomei Xu<sup>ID</sup>, and Aijun Song, *Member, IEEE*

**Abstract**—Frequency-domain equalization (FDE) is a computationally efficient method to recover underwater acoustic single-carrier transmissions in a multipath environment. The FDE receivers often operate in a block-by-block manner, assuming that the channel is time invariant during a block duration. This assumption implies that traditional block-based FDE receivers experience performance degradation in fast time-varying channel conditions, since the **interfrequency interference (IFI)** is often not considered. Here, we focus on the **IFI cancellation (IFIC)** in single-carrier transmissions. The IFI formulations are developed for a blockwise FDE receiver, where the time reversal (TR) processing is incorporated to alleviate the interblock interference. Based on the formulations, the IFI is estimated by the time-varying impulse responses, which are obtained from an adaptive basis expansion model. A soft two-step IFIC strategy is then employed to address the **IFI**. In the first step, the main IFI is removed by the time-varying TR processing and explicit IFI cancellation. The residual IFI is suppressed by the frequency-domain decision feedback equalization (FD-DFE) in the second step. To further enhance the communication performance, we develop a **soft-symbol-based iterative receiver, referred to as IFIC-FD-DFE**. The impulse responses, explicit IFI, and residual IFI are updated in an iterative fashion, based on the soft symbol estimates. The proposed receiver has been tested using the at-sea measurements collected at the Gulf of Mexico in August 2017. Communication packets at four ranges at the carrier frequency of 160 kHz with a symbol rate of 32 kHz have been decoded. The effectiveness of the IFIC-FD-DFE receiver has been demonstrated via comparisons with several FDE schemes in the current literature.

**Index Terms**—Decision feedback equalization (DFE), frequency-domain equalization (FDE), interfrequency interference (IFI), underwater acoustic (UWA) communications.

### NOMENCLATURE

$n$	Time instant.
$k$	Frequency bin index.
$\mathbb{C}$	Complex set.
*	Linear convolution.
$ \cdot $	Modulus of a complex number.
$E[\cdot]$	Expectation operation.
$\text{Re}\{\cdot\}/\text{Im}\{\cdot\}$	Real/imaginary values.

Manuscript received April 18, 2019; revised December 9, 2019 and April 24, 2020; accepted June 1, 2020. Date of publication July 14, 2020; date of current version April 14, 2021. This work was supported in part by the National Natural Science Foundation of China under Grants 41676024 and 41976178, in part by China Scholarship Council (Student 201606310159), in part by the U.S. National Science Foundation (CNS 1801861), and in part by the Department of the Treasury through the State of Texas under the Resources and Ecosystems Sustainability, Tourist Opportunities, and Revived Economies of the Gulf Coast States Act of 2012 (RESTORE Act). (Corresponding author: Xiaomei Xu.)

**Associate Editor:** L. Culver.

Xingbin Tu and Xiaomei Xu are with the Key Lab of Underwater Acoustic Communication and Marine Information Technology and the College of Ocean & Earth Sciences, Xiamen University, Xiamen 361102, China (e-mail: xbtu@stu.xmu.edu.cn; xmxu@xmu.edu.cn).

Aijun Song is with the Department of Electrical and Computer Engineering, University of Alabama, Tuscaloosa, AL 35401 USA (e-mail: song@eng.ua.edu). Digital Object Identifier 10.1109/JOE.2020.3000319

$F_N$	$N \times N$ discrete Fourier transform matrix.
$\mathbf{0}_N$	All-zero vector of length $N$ .
$\hat{(\cdot)}$	Variables in zero-padding blocks.
$(\cdot)$	Variables after TR processing.
$\hat{(\cdot)}$	Estimated variables.
$\bar{(\cdot)}$	Soft symbol for $s$ ( $\mathcal{S}$ ), or average for other variables.
$(\cdot)^T / (\cdot)^H$	Transpose/Hermitian transpose.
$(\cdot)_{[a:b]}$	Subvector from index $a$ to $b$ .
$(\cdot)_{[a:b,c:d]}$	Submatrix from row $a$ to $b$ and column $c$ to $d$ .
$\text{diag}\{a_1, \dots, a_N\}$	Diagonal matrix with elements $a_1, \dots, a_N$ .
$s, r, \eta, h$	Time-domain vectors.
$A, H, Q$	Time-domain matrix.
$\{\mathcal{H}, \mathcal{Q}, \mathcal{W}$	Frequency-domain matrices/vectors.
$\{\mathcal{S}, \mathcal{R}, \mathcal{N}, \mathcal{I}, \mathcal{X}$	

### I. INTRODUCTION

THE underwater acoustic (UWA) channel is a time-varying multipath environment [1]. The multipath propagation leads to the intersymbol interference (ISI) at the receiver. For single-carrier transmissions, blockwise frequency-domain equalization (FDE) [2]–[4] is a low-complexity technique to address the ISI. If FDE is utilized in the fast time-varying UWA channel, the interfrequency interference (IFI) is induced to the receivers. After FDE, the IFI leads to the residual interference [5], which cannot be removed by the linear equalization. In this article, we address this issue in the FDE receiver for the fast time-varying channel.

To address the IFI resulted from fast channel variability, an implicit solution, decision feedback equalization (DFE) [6], has been incorporated in FDE receivers. The IFI is manifested in the form of residual interference, which is estimated by the symbol decision and is removed in the iterative receiver. Two types of DFEs, time-domain DFE (TD-DFE) [7]–[10] and frequency-domain DFE (FD-DFE) [11]–[15], were studied. In the TD-DFE receiver, multichannel feedforward filters operate in the frequency domain, whereas the single-channel feedback filter performs in the time domain. This receiver exploits the limited bandwidth of the transmitted signal to reduce the number of estimated parameters. In the FD-DFE receiver, both the feedforward and feedback filters perform in the frequency domain. Prefixes are often inserted among blocks to avoid the interblock interference (IBI). In this article, we focus on the FD-DFE receiver.

The FD-DFE method was applied in both wireless radio-frequency [11]–[13] and UWA [14]–[16] environments. In the wireless radio-frequency environment, the **FD-DFE receiver was often conducted based on the soft symbol estimates**. Performance gains were achieved in comparison with the hard-symbol-based counterpart [11], [12]. The performance of FD-DFE is also affected by the channel

estimation accuracy. The power of channel estimation errors, however, can alleviate the performance degradation [13]. In the UWA environment, the FD-DFE receiver exhibited better performance than the linear FDE receiver [14]. A simplified version based on the preset signal-to-noise ratio (SNR) and symbol error rate limit was developed to reduce the receiver complexity [15]. These preset parameters, however, were not always optimal in fast time-varying channels.

Turbo equalization [10], [16]–[18] was studied to enhance the receiver performance for these two types of DFE receivers. In [17], turbo equalization was integrated in the block TD-DFE receiver. In [10], iterative equalization was incorporated in an FD-DFE receiver. Better performance was demonstrated in both cases. The frequency-domain turbo equalization was developed for the multiple-input–multiple-output system in the UWA environment [18].

Explicit IFI cancellation has been investigated in the UWA orthogonal frequency division multiplexing (OFDM) [5], [19], [20] and wireless radio-frequency [21]–[24] systems. In the UWA OFDM systems, the IFI is addressed in the form of intercarrier interference (ICI). It was estimated by an iterative receiver, and was addressed in the iterations [5], [19]. Besides, the basis expansion model (BEM) was applied for explicit ICI cancellation in OFDM systems [20]. In the wireless radio-frequency environment, the IFI was also calculated in an iterative fashion [21], [22]. The IFI was then canceled in the time domain [23] or in frequency domain [24]. So far, explicit IFI cancellation has not been studied in UWA single-carrier systems.

This article focuses on the IFI cancellation for single-carrier transmissions. The contributions are summarized as follows. **First, we develop the formulation of the IFI in the UWA single-carrier transmissions.** The IFI, resulted from channel variations within one processing block, is calculated in the general zero-padding FDE receiver. In traditional FDE receivers, this term is omitted by assuming a static channel condition within one processing block, or is implicitly addressed together with the ISI. The formulated IFI is extended to a blockwise FDE receiver based on the time reversal (TR) processing.

**Second, we propose a soft two-step IFIC method to address the IFI.** In the first step, a time-varying TR (TVTR) processing and a soft IFIC method are conducted to remove the main IFI. In the second step, the residual IFI estimate is fed back for IFI cancellation in the FD-DFE structure. In both steps, the IFIs are estimated by the soft symbol estimates and the  $q$ -function, latter of which is also obtained from the soft symbol estimates.

**Third, we develop a soft-symbol-based iterative receiver, referred to as IFIC-FD-DFE.** In this receiver, three set of receiver outputs, the channel estimates from an BEM estimator, the explicit IFI estimates from IFIC, and the residual IFI estimates from FD-DFE, are iteratively updated based on the soft symbol estimates. Furthermore, the adaptive BEM estimator is used. The basis number is dynamically adjusted according to the instant channel variability, rather than a fixed value. With these features, the receiver performance is greatly improved.

The IFIC-FD-DFE receiver uses a TR processor, which is a shared feature with our previously published FDE receiver [25]. The TR processor is useful here to achieve the blockwise FD-DFE. Due to the low-power sidelobes of the  $q$ -function, the IBI can be suppressed. The complexity is also reduced as the multichannel signals are converted into a single composite signal. It is noted that our TR-based FDE receiver in [25] does not address the IFI. To alleviate the IFI caused by fast channel fluctuations, we extend the TR processor to a time-varying version, referred to as the TVTR processor. It directly uses the BEM coefficients to reduce the complexity when computing the  $q$ -function in a symbol-by-symbol fashion. This TVTR processor is different from the scheme in [26], which applies the TR combining in the sparse delay-Doppler plane.

High-rate transmissions at the acoustic carrier frequency of 160 kHz were carried out in an at-sea experiment at the Gulf of Mexico. Due to the high-frequency acoustic transmissions in the dynamic environment, the channel impulse responses exhibited fast fluctuations. With the proposed algorithms, communication packets at four ranges were decoded in the fast time-varying channel conditions. The receiver showed performance gains over the FD-DFE or multichannel DFE receivers, which do not addressed the IFI explicitly.

The rest of this article is organized as follows. Section II briefly introduces the communication system model. The IFI in the FDE receiver is formulated. Section III details the proposed blockwise IFIC-FD-DFE receiver. Experimental results and discussions are presented in Section IV. Section V concludes this article.

## II. IFI IN FDE RECEIVER

In this section, we derive the formulations related to the IFI for the UWA signal-carrier transmissions. A single-input and multiple-output communication system is considered. We first consider zero-padding blocks. It can be extended to the FDE receiver based on the TR processing.

In the communication system, the received signal is modeled as the convolution between the transmitted signal and the time-varying channel impulse response, with added ambient noise. Let  $N$  denote the total number of the symbols in one block and  $L$  denote the channel length. We use

$$\mathbf{s} = [s(0), s(1), \dots, s(N-1)]^T$$

and

$$\mathbf{r}_m = [r_m(0), r_m(1), \dots, r_m(N-1)]^T$$

to represent the transmitted sequence and the corresponding received signal at the  $m$ th hydrophone, respectively. The vectors

$$\dot{\mathbf{s}} = [\mathbf{s}^T, \mathbf{0}_{L-1}^T]^T$$

and

$$\dot{\mathbf{r}}_m = [\mathbf{r}_m(0), \mathbf{r}_m(1), \dots, \mathbf{r}_m(N+L-2)]^T$$

represent the zero-padded transmitted signal and the corresponding received signal, respectively.

The zero-padded received signal  $\dot{\mathbf{r}}_m$  can be expressed as

$$\dot{\mathbf{r}}_m = \dot{\mathbf{H}}_m \dot{\mathbf{s}} + \dot{\eta}_m \quad (1a)$$

where  $\dot{\eta}_m = [\eta_m(0), \eta_m(1), \dots, \eta_m(N+L-2)]^T$  is the additive white Gaussian noise and  $\dot{\mathbf{H}}_m$  is the channel matrix between the transmitter and the  $m$ th hydrophone. The channel matrix  $\dot{\mathbf{H}}_m$  is defined in (1b), shown at the bottom of the next page, where  $h_m(n, l)$  is the  $l$ th ( $l = 0, \dots, L-1$ ) path gain at instant  $n$  at the  $m$ th hydrophone. Channel matrix  $\dot{\mathbf{H}}_m$  can be decomposed into the time-invariant part  $\dot{\mathbf{H}}_{m,i}$  and the time-variant part  $\dot{\mathbf{H}}_{m,v}$ , both of which share a similar structures with  $\dot{\mathbf{H}}_m$ . The element  $h_m(n, l)$  becomes  $h_{m,i}(l) = 1/(N+L-1) \sum_{n=0}^{N+L-2} h_m(n, l)$  in  $\dot{\mathbf{H}}_{m,i}$ , and  $h_{m,v}(n, l) = h_m(n, l) - h_{m,i}(l)$  in  $\dot{\mathbf{H}}_{m,v}$ . Thus, we can write (1a) as

$$\dot{\mathbf{r}}_m = \dot{\mathbf{H}}_{m,i} \dot{\mathbf{s}} + \dot{\mathbf{H}}_{m,v} \dot{\mathbf{s}} + \dot{\eta}_m. \quad (2a)$$

Its frequency-domain expression is

$$\dot{\mathcal{R}}_m = \dot{\mathcal{H}}_{m,i} \dot{\mathcal{S}} + \mathbf{F}_{N+L-1} \dot{\mathbf{H}}_{m,v} \dot{\mathbf{s}} + \dot{\mathcal{N}}_m \quad (2b)$$

where  $\dot{\mathcal{R}}_m = \mathbf{F}_{N+L-1} \dot{\mathbf{r}}_m$ ,  $\dot{\mathcal{H}}_{m,i} = \mathbf{F}_{N+L-1} \dot{\mathbf{H}}_{m,i} \mathbf{F}_{N+L-1}^H$ ,  $\dot{\mathcal{S}} = \mathbf{F}_{N+L-1} \dot{\mathbf{s}}$ , and  $\dot{\mathcal{N}}_m = \mathbf{F}_{N+L-1} \dot{\eta}_m$ .  $\dot{\mathcal{H}}_{m,i}$  is a diagonal matrix since  $\dot{\mathbf{H}}_{m,i}$  is a circulant matrix.

The first term in (2b) denotes the ISI induced by multipath propagation. The second term denotes the IFI induced by the channel variation, i.e.,

$$\mathcal{I} = \mathbf{F}_{N+L-1} \mathring{\mathbf{H}}_{m,v} \mathring{\mathbf{s}}. \quad (3)$$

It can also be expressed as

$$\mathcal{I} = \mathring{\mathcal{H}}_{m,v} \mathring{\mathbf{s}} \quad (4)$$

where  $\mathring{\mathcal{H}}_{m,v} = \mathbf{F}_{N+L-1} \mathring{\mathbf{H}}_{m,v} \mathbf{F}_{N+L-1}^H$  is an off-diagonal matrix. The IFI intensity depends on the Frobenius norm of  $\mathring{\mathbf{H}}_{m,v}$ , i.e., the channel variability.

The above expressions are readily extended to the TR-based FDE receiver. In the TR-based receiver, the multichannel impulse responses are combined into a composite single-channel  $q$ -function  $\mathbf{Q}$  by the TR processing. The  $N \times N$  matrix  $\mathbf{Q}$  is a Toeplitz-like matrix. Its first row is given as

$$[q(0, 0), \dots, q(0, -L + 1), 0, \dots, q(0, L - 1), \dots, q(0, 1)]$$

and the first column is given as

$$[q(0, 0), \dots, q(L - 1, L - 1), 0, \dots, q(N - L + 1, -L + 1), \dots, q(N - 1, -1)]^T.$$

Likewise, the multichannel signals and noise terms are converted to the single-channel signal  $\mathring{\mathbf{R}}$  and noise term  $\mathcal{N}$ , i.e.,

$$\mathring{\mathbf{R}} = \mathcal{Q}_i \mathbf{S} + \mathbf{F}_N \mathbf{Q}_v \mathbf{s} + \mathcal{N} \quad (5)$$

where  $\mathcal{Q}_i$  is the frequency-domain transformation of the time-invariant component of the  $q$ -function and  $\mathbf{Q}_v$  is the time-variant part. Thus, the IFI in our TR-based FDE receiver is

$$\mathcal{I} = \mathbf{F}_N \mathbf{Q}_v \mathbf{s}. \quad (6)$$

The details of TR processing will be shown in Section III-B.

### III. IFIC-FD-DFE RECEIVER

In this section, we present the IFIC-FD-DFE receiver based on the adaptive BEM estimator. The complexity of the proposed receiver is analyzed in comparison with two types of related receiver structures, the FDE and FD-DFE receivers. The FDE receiver here refers to the overlapping FDE scheme based on the TR processing [25]. The FD-DFE receiver is extended from the FDE receiver by replacing the FDE with FD-DFE.

The IFIC-FD-DFE receiver is illustrated in Fig. 1, with three main procedures, the adaptive BEM, TVTR processing, and IFIC-FD-DFE. These three procedures will be explained in detail in Sections III-A, III-B, and III-C.

$$\mathring{\mathbf{H}}_m = \begin{bmatrix} h_m(0, 0) & & & & h_m(0, L - 1) & \cdots & h_m(0, 1) \\ h_m(1, 1) & \ddots & & & \ddots & & \vdots \\ \vdots & \vdots & \ddots & & & & \\ h_m(L - 1, L - 1) & \vdots & & \ddots & & & h_m(L - 2, L - 1) \\ & \ddots & & \vdots & & & \vdots \\ & & h_m(N + L - 2, L - 1) & & \cdots & & h_m(N + L - 2, 0) \end{bmatrix} \in \mathbb{C}^{(N+L-1) \times (N+L-1)} \quad (1b)$$

In the receiver, first, the received signal from  $M$  hydrophones,  $\mathbf{r}_m$ ,  $m = 1, 2, \dots, M$ , are used to estimate the impulse responses based on the adaptive BEM estimator. Next, the received signal from all the hydrophones are processed by the TVTR processing. The  $q$ -function matrix  $\mathbf{Q}$  and time-reversed signal  $\mathring{\mathbf{R}}$  are obtained. Afterward, a two-step IFIC-FD-DFE is conducted. The IFI estimate  $\hat{\mathcal{I}}$  is removed from  $\mathring{\mathbf{R}}$  in the first step, yielding the IFI-canceled signal  $\mathbf{X}$ . The ISI and residual IFI  $\hat{\mathcal{I}}_r$  are then eliminated by FD-DFE in the second step, yielding the soft symbol estimate  $\bar{\mathbf{s}}$  of the transmitted sequence.

#### A. Adaptive BEM

We use the adaptive BEM to estimate the time-varying impulse responses. In this section, we derive the BEM and its adaptive version for the single-carrier system. The latter dynamically adjusts the basis number of the BEM according to the instant channel variability. The first and last  $L - 1$  symbols of the variable  $\mathbf{r}$  in (1) are not considered because of the IBI. For the sake of simplicity, we drop the hydrophone subscript  $m$  in (1).

We use the complex exponential basis  $\{e^{j2\pi\omega n/N}\}_{\omega=-(\Omega-1)/2}^{(\Omega-1)/2}$  to approximate the channel variation. Note that the number of the bases  $\Omega$  is an odd integer. The tap coefficient  $h(n, l)$  of the channel matrix is expressed as

$$h(n, l) = \sum_{\omega=-(\Omega-1)/2}^{(\Omega-1)/2} \gamma_{\omega,l} e^{j2\pi\omega(n-l)/N} \quad (7)$$

where  $\gamma_{\omega,l}$  is the BEM coefficient for basis  $\omega$ .

We use  $\mathbf{H}_{[L:N,1:N]}$  to represent a submatrix of  $\mathring{\mathbf{H}}_m$ . The submatrix  $\mathbf{H}_{[L:N,1:N]}$  can be expressed as

$$\mathbf{H}_{[L:N,1:N]} = \sum_{\omega=-(\Omega-1)/2}^{(\Omega-1)/2} \boldsymbol{\Gamma}_\omega \mathbf{E}_\omega \quad (8)$$

where

$$\mathbf{E}_\omega = \text{diag}\{1, e^{j2\pi\omega/N}, \dots, e^{j2\pi\omega(N-1)/N}\}.$$

The  $(N - L + 1) \times N$  matrix  $\boldsymbol{\Gamma}_\omega$  is a nonsymmetric Toeplitz matrix. Its first row is given as  $[\gamma_{\omega,L-1}, \gamma_{\omega,L-2}, \dots, \gamma_{\omega,0}, 0, \dots, 0]$ , and the first column is given as  $[\gamma_{\omega,L-1}, 0, \dots, 0]^T$ .

Thus, the subvector of the received signal vector  $\mathbf{r}_m$  in (1a),  $\mathbf{r}_{[L:N]}$ , can be expressed as

$$\mathbf{r}_{[L:N]} = \sum_{\omega=-(\Omega-1)/2}^{(\Omega-1)/2} \mathbf{A}_\omega \boldsymbol{\gamma}_\omega + \boldsymbol{\eta}_{[L:N]} \quad (9a)$$

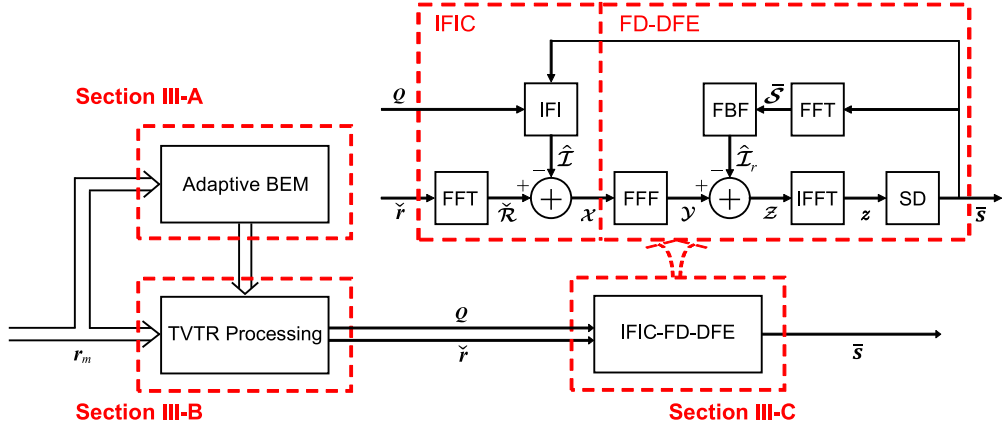


Fig. 1. IFIC-FD-DFE receiver for UWA single-carrier transmissions. FFF = feedforward filter, FBF = feedback filter, FFT = fast Fourier transform, IFFT = inverse FFT, and SD = soft decision.

where  $\gamma_\omega = [\gamma_{\omega,0}, \gamma_{\omega,1}, \dots, \gamma_{\omega,L-1}]^T$ , and

$$\mathbf{A}_\omega = \begin{bmatrix} s_\omega(L-1) & s_\omega(L-2) & \cdots & s_\omega(0) \\ s_\omega(L) & s_\omega(L-1) & \cdots & s_\omega(1) \\ \vdots & \vdots & \ddots & \vdots \\ s_\omega(N-1) & s_\omega(N-2) & \cdots & s_\omega(N-L) \end{bmatrix} \in \mathbb{C}^{(N-L+1) \times L} \quad (9b)$$

with  $s_\omega(n) = \mathcal{E}_\omega(n)s(n)$ . In the training blocks, the transmitted symbol  $s(n)$  is known to the receiver. In the data blocks,  $s(n)$  should be replaced with the normalized soft symbol estimate  $\bar{s}(n)/(\sum_{n=0}^{N-1} |\bar{s}(n)|^2/N)^{1/2}$ . Thus, (9) can be rewritten in a matrix form as

$$\mathbf{r}_{[L:N]} = \mathbf{A}\gamma + \boldsymbol{\eta}_{[L:N]} \quad (10)$$

where

$$\mathbf{A} = [\mathbf{A}_{-(\Omega-1)/2}, \dots, \mathbf{A}_{(\Omega-1)/2}] \in \mathbb{C}^{(N-L+1) \times \Omega L}$$

and

$$\gamma = [\gamma_{-(\Omega-1)/2}^T, \dots, \gamma_{(\Omega-1)/2}^T]^T \in \mathbb{C}^{\Omega L \times 1}.$$

We adopt a sparse channel estimation method, the compressive sampling matching pursuit (CoSaMP), to solve (10), since the acoustic channel is often sparse. One may refer to [27] for the algorithm details. Once  $\gamma$  is obtained, the time-varying impulse response estimates can be calculated with (7).

The choice of  $\Omega$  depends on the channel fluctuation rate in the data block, i.e., on the Doppler spread or coherence time [28], [29]. Based on [28] and [29, eq. (2.103)], we derive  $\Omega$  as a function of coherence time  $t_c$

$$\Omega = 2 \left\lceil \frac{0.413 N}{\pi R_s t_c} \right\rceil + 1 \quad (11)$$

where  $R_s$  is the symbol rate. Note that  $t_c$  is defined as the duration for which the correlation coefficient drops below 0.7 here.

The adaptive BEM estimator is presented in Algorithm 1. It estimates the impulse responses in an iterative fashion for each data block at each hydrophone channel. First, at each data block, it calculates the coherence time  $t_c$  based on the impulse responses. At the beginning of a packet, we use  $b_{\text{lag}}$  blocks as the training blocks to estimate the initial correlation coefficients of channels. Second, we choose a

---

**Algorithm 1:** Adaptive BEM in One Block for the  $m$ th Channel.

---

**Input:**  $\mathbf{r}, \mathbf{A}, N, R_s$ , current iteration  $\psi$ , total iterations  $\Psi$

**Output:**  $\hat{h}_m(n, l)$

**for**  $\psi = 1$  to  $\Psi$  **do**

  1) Calculate  $t_c$ ;

  2) Choose

$$\Omega = \begin{cases} 1, & \frac{0.413 N}{\pi R_s t_c} \leqslant 0.05 \\ 2 \left\lceil \frac{0.413 N}{\pi R_s t_c} \right\rceil + 1, & \frac{0.413 N}{\pi R_s t_c} > 0.05 \end{cases};$$

  3) **if**  $\psi = 1$  **then**

    | calculate  $\hat{h}_m(n, l)$  of previous block with  $\Omega = 1$ ;

**else**

    | calculate  $\hat{h}_m(n, l)$  of current block with the chosen  $\Omega$ ;

**end**

**end**

---

proper number for  $\Omega$  according to (11). To include  $\Omega = 1$ , we set the corresponding upper limit of  $0.413 N/(\pi R_s t_c)$  as 0.05. Finally, the BEM algorithm generates the impulse response estimates. In the first iteration, it calculates the impulse responses of the previous block with  $\Omega = 1$ . In the rest iterations, the estimator calculates  $\hat{h}_m(n, l)$  of the current block with a chosen  $\Omega$ .

## B. TVTR Processing

The multichannel signals from all sensors are combined by the TVTR processor as

$$\begin{aligned} \check{r}(n) &= \sum_{m=1}^M r_m(n) * \bar{h}_m^*(L-1-l) \\ &= q(n, l') * s(n) + \check{\eta}(n) \end{aligned} \quad (12a)$$

where  $\bar{h}_m(l)$  is the averaged impulse response,  $q(n, l')$  is the time-varying  $q$ -function with  $l' = -L+1, \dots, 0, \dots, L-1$ , and  $\check{\eta}(n)$  is

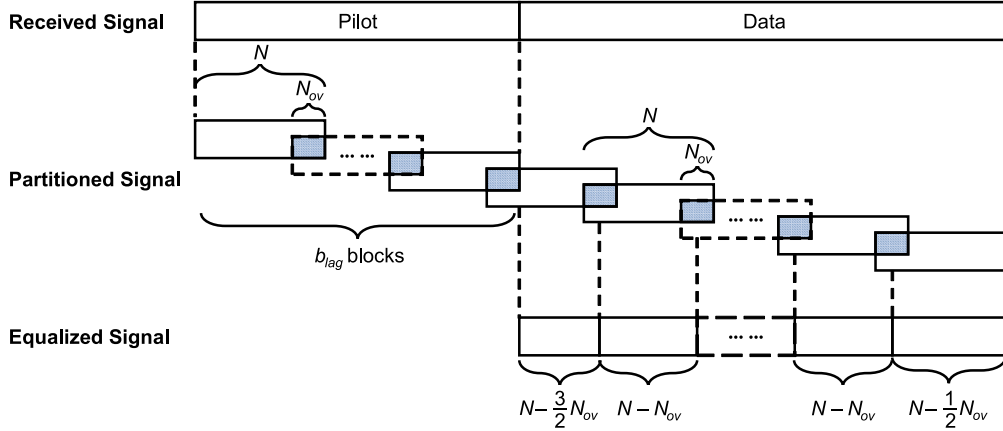


Fig. 2. Overlapping block partitioning.

the noise component. They are obtained as

$$\begin{aligned} \bar{h}_m(l) &= \frac{1}{N} \sum_{n=0}^{N-1} \hat{h}_m(n, l) \\ q(n, l') &= \sum_{m=1}^M h_m(n, l) * \bar{h}_m^*(L-1-l) \\ \check{\eta}(n) &= \sum_{m=1}^M \eta_m(n) * \bar{h}_m^*(L-1-l) \end{aligned} \quad (12b)$$

where  $\hat{h}_m(n, l)$  is the estimated impulse response. The  $q$ -function in (12b) can be calculated based on (7) to achieve reduced complexity, i.e.,

$$\begin{aligned} q(n, l') &= \sum_{m=1}^M \sum_{\omega=-(\Omega-1)/2}^{(\Omega-1)/2} e^{j2\pi\omega n/N} \\ &\times ((\gamma_{m,\omega} e^{-j2\pi\omega l/N}) * \bar{h}_m^*(L-1-l)). \end{aligned} \quad (12c)$$

The TR output in (12) can be written in the matrix form as

$$\begin{aligned} \check{\mathbf{r}} &= \sum_{m=1}^M \bar{\mathbf{H}}_m \check{\mathbf{r}}_m \\ &= \sum_{m=1}^M \bar{\mathbf{H}}_m (\mathbf{H}_m \check{\mathbf{s}} + \check{\eta}_m) \\ &= \check{\mathbf{Q}} \check{\mathbf{s}} + \check{\eta} \end{aligned} \quad (13a)$$

where

$$\check{\mathbf{r}} = [\check{r}(0), \dots, \check{r}(N-1)]^T, \check{\mathbf{s}} = [s(-L+1), \dots, s(N+L-2)]^T$$

and

$$\check{\eta} = [\check{\eta}(0), \dots, \check{\eta}(N-1)]^T.$$

In (13a), matrices  $\mathbf{H}_m$ ,  $\bar{\mathbf{H}}_m$ , and  $\check{\mathbf{Q}}$  are organized as follows:

$\mathbf{H}_m$

$$\begin{aligned} &= \begin{bmatrix} h_m(0, L-1) & \cdots & h_m(0, 0) \\ & \ddots & \ddots \\ h_m(N+L-2, L-1) & \cdots & h_m(N+L-2, 0) \end{bmatrix} \\ &\in \mathbb{C}^{(N+L-1) \times (N+2L-2)} \end{aligned} \quad (13b)$$

$$\begin{aligned} \bar{\mathbf{H}}_m &= \begin{bmatrix} \bar{h}_m^*(0) & \cdots & \bar{h}_m^*(L-1) \\ \ddots & \ddots & \ddots \\ \bar{h}_m^*(0) & \cdots & \bar{h}_m^*(L-1) \end{bmatrix} \\ &\in \mathbb{C}^{N \times (N+L-1)} \end{aligned} \quad (13c)$$

$$\begin{aligned} \check{\mathbf{Q}} &= \sum_{m=1}^M \bar{\mathbf{H}}_m \mathbf{H}_m \\ &= \begin{bmatrix} q(0, L-1) & \cdots & q(0, -L+1) \\ \ddots & \ddots & \ddots \\ q(N-1, L-1) & \cdots & q(N-1, -L+1) \end{bmatrix} \\ &\in \mathbb{C}^{N \times (N+2L-2)}. \end{aligned} \quad (13d)$$

It is shown in (13) that the precursor and postcursor interferences are both included in the current block. If we discard them, and replace  $\check{\mathbf{Q}}$  and  $\check{\mathbf{s}}$  with  $\mathbf{Q}$  and  $\mathbf{s}$ , (13) is approximated by

$$\check{\mathbf{r}} \approx \mathbf{Q} \mathbf{s} + \check{\eta}. \quad (14)$$

There are two ways to reduce the approximation error induced by the IBI. One way is the TR processing. Since the power of sidelobes is much lower than that of the mainlobe, or the peak, the precursor and postcursor interferences are suppressed after the TR processing. The other way is the overlapping partitioning, as shown in Fig. 2. The successive signal is first partitioned into overlapping blocks with an overlapping rate  $\beta = N_{ov}/N \times 100\%$ , where  $N_{ov}$  is the number of overlapping symbols. Zero padding may be required for the last block. After equalization, first and last  $N_{ov}/2$  symbols are discarded to mitigate the impact of the precursor and postcursor interferences.

### C. IFI-Cancelation-Based Frequency-Domain Decision Feedback Equalization (IFIC-FD-DFE)

IFIC-FD-DFE is the core procedure, as the interferences, including the ISI, IFI, and residual IFI, are mitigated iteratively in this procedure. According to (6), the IFI is estimated by

$$\hat{\mathcal{I}} = \mathbf{F}_N \mathbf{Q}_v \bar{\mathbf{s}} \quad (15a)$$

where  $\bar{\mathbf{s}} = [\bar{s}(0), \dots, \bar{s}(N-1)]^T$  and  $\mathbf{Q}_v$  has a similar structure as  $\mathbf{Q}$ , with its element

$$q_v(n, l') = q(n, l') - q_i(l'). \quad (15b)$$

In (15b), the time-invariant  $q$ -function is

$$q_i(l') = \sum_{m=1}^M \bar{h}_m(l) * \bar{h}_m^*(L-1-l). \quad (15c)$$

The soft symbol estimate  $\bar{s}$  is calculated under the additive white Gaussian assumption [30]. For quadrature phase-shift keying (QPSK) modulations, the log-likelihood ratios (LLRs) of the in-phase and quadrature coordinates in one symbol are, respectively, given by

$$L_1(n) = \frac{\sqrt{8}\operatorname{Re}\{z(n)\}}{\sigma^2}, \quad L_2(n) = \frac{\sqrt{8}\operatorname{Im}\{z(n)\}}{\sigma^2} \quad (16)$$

where  $z(n)$  is the equalized signal and  $\sigma^2$  is the noise variance given by

$$\begin{aligned} \sigma^2 &= E[|z(n) - s(n)|^2] \\ &\approx \frac{1}{N} \sum_{n=0}^{N-1} |z(n) - \hat{s}(n)|^2 \end{aligned} \quad (17)$$

with the hard decision

$$\hat{s}(n) = (\operatorname{sgn}(\operatorname{Re}\{z(n)\}) + j\operatorname{sgn}(\operatorname{Im}\{z(n)\}))/\sqrt{2}.$$

The soft symbol estimate is obtained with the LLRs

$$\bar{s}(n) = \frac{1}{\sqrt{2}} \left[ \tanh\left(\frac{L_1(n)}{2}\right) + j\tanh\left(\frac{L_2(n)}{2}\right) \right]. \quad (18)$$

In the first iteration,  $\bar{s}(n) = 0$ .

After IFI cancelation by

$$\mathcal{X} = \check{\mathcal{R}} - \hat{\mathcal{I}} \quad (19)$$

the equalized signal is obtained by FD-DFE

$$\begin{aligned} \mathcal{Z} &= \mathcal{Y} - \hat{\mathcal{I}}_r \\ &= \mathcal{W}\mathcal{X} - \hat{\mathcal{I}}_r \end{aligned} \quad (20)$$

where  $\hat{\mathcal{I}}_r$  is the residual IFI, and  $\mathcal{W}$  is the weight matrix for a feedforward filter. As the IFI has been suppressed, we can treat the channel as time invariant. Thus,  $\mathcal{W}$  is simplified to a diagonal matrix with its  $k$ th diagonal element being  $\mathcal{W}(k)$ . Therefore, (20) is simplified to

$$\mathcal{Z}(k) = \mathcal{W}(k)\mathcal{X}(k) - \hat{\mathcal{I}}_r(k) \quad (21a)$$

where

$$\mathcal{X}(k) = \mathcal{Q}_i(k)\mathcal{S}(k) + \mathcal{N}(k). \quad (21b)$$

The mean square error of the equalized signal is

$$\begin{aligned} \zeta &= E[|z(n) - s(n)|^2] \\ &= E[|\mathcal{Z}(k) - \mathcal{S}(k)|^2]. \end{aligned} \quad (22)$$

Substituting (21) into (22) yields

$$\begin{aligned} \zeta &= E[|\mathcal{W}(k)[\mathcal{Q}_i(k)\mathcal{S}(k) + \mathcal{N}(k)] - \hat{\mathcal{I}}_r(k) - \mathcal{S}(k)|^2] \\ &= \frac{1}{N} \sum_{k=0}^{N-1} \left\{ |\mathcal{W}(k)\mathcal{Q}_i(k) - 1|^2 E[|\mathcal{S}(k)|^2] \right. \\ &\quad + |\hat{\mathcal{I}}_r(k)|^2 + |\mathcal{W}(k)|^2 E[|\mathcal{N}(k)|^2] \\ &\quad \left. - 2\operatorname{Re}\{[\mathcal{W}(k)\mathcal{Q}_i(k) - 1]\mathcal{S}(k)\hat{\mathcal{I}}_r^*(k)\} \right\}. \end{aligned} \quad (23)$$

By setting to zero the gradient of  $\zeta$  with respect to  $\hat{\mathcal{I}}_r$  and by replacing the unavailable ground truth  $\mathcal{S}(k)$  with the soft symbol estimate  $\bar{\mathcal{S}}(k)$ , we obtain the residual IFI

$$\hat{\mathcal{I}}_r(k) = [\mathcal{W}(k)\mathcal{Q}_i(k) - 1]\bar{\mathcal{S}}(k). \quad (24)$$

Substituting (24) into (23) and setting to zero the gradient of  $\zeta$  with respect to  $\mathcal{W}$  yield

$$\mathcal{W}(k) = \varrho\mathcal{G}(k) \quad (25a)$$

with

$$\begin{aligned} \mathcal{G}(k) &= \frac{\mathcal{Q}_i^*(k)}{(1 - \lambda_{\psi-1}^2)|\mathcal{Q}_i(k)|^2 + E[|\mathcal{N}(k)|^2]/E[|\mathcal{S}(k)|^2]} \\ \varrho &= N \left[ \sum_{k=0}^{N-1} \mathcal{G}(k)\mathcal{Q}_i(k) \right]^{-1} \end{aligned} \quad (25b)$$

where  $\lambda_{\psi}$  is the decision reliability in the  $\psi$ th iteration. It is calculated by

$$\lambda_{\psi} = \frac{1}{2N} \sum_{n=0}^{N-1} (\lambda_1(n) + \lambda_2(n)) \quad (26a)$$

where  $\lambda_1(n)$  and  $\lambda_2(n)$  are the reliabilities of the soft symbol coordinates

$$\begin{aligned} \lambda_1(n) &= \tanh\left(\frac{|L_1(n)|}{2}\right) \\ \lambda_2(n) &= \tanh\left(\frac{|L_2(n)|}{2}\right). \end{aligned} \quad (26b)$$

In the first iteration,  $\lambda_{\psi} = 0$ .

#### D. Iterative Processing

The iterative processing for an individual block is illustrated in Fig. 3. The iteration counting variable  $\psi$  is initialized to zero, and the soft symbol estimate  $\bar{s}$  is initialized to a zero vector. First, the impulse responses  $\hat{h}_m(n, l)$  ( $m = 1, \dots, M$ ) are estimated by the adaptive BEM as in Section III-A. After the TVTR processing (see Section III-B), the  $q$ -function is forwarded for IFI cancelations. In the first iteration, traditional FDE is conducted. The IFI is not considered at this stage. In the rest iterations, the explicit IFI estimates  $\hat{\mathcal{I}}$  and the residual IFI estimates  $\hat{\mathcal{I}}_r$  are sequentially canceled in the IFIC and FD-DFE structures as in Section III-C. The processing advances to the next iteration if the total iteration count  $\Psi$  has not been reached.

In the iterations, the three sets of receiver outputs,  $\hat{h}_m(n, l)$ ,  $\hat{\mathcal{I}}$ , and  $\hat{\mathcal{I}}_r$ , are iteratively updated based on the soft symbol estimates  $\bar{s}$ . These outputs, in turn, make the soft symbol estimates more reliable in the iterations. The receiver performance is then greatly improved with the iterative processing.

#### E. Complexity Analysis

We compare the computational costs of the FDE, FD-DFE, and IFIC-FD-DFE schemes. The details are listed in Table I. For  $\psi = 1$ , all schemes have the same complexity. They all use the TR-based FDE in the first iteration. For  $\psi > 1$ , the complexity of FD-DFE and IFIC-FD-DFE becomes larger as feedback branches are included. Channel estimation dominates the computational complexity. If the BEM estimator is used, the complexity is proportional to the number of the BEM bases. The TVTR processing in IFIC-FD-DFE also introduces additional complexity. In the rest operations, the complexity is independent of the receiving element number, as the receiver uses the

TABLE I  
COMPLEXITY COMPARISON AMONG THE FDE, FD-DFE, AND IFIC-FD-DFE SCHEMES. (A) COMPLEXITY FOR  $\psi = 1$  AND (B) COMPLEXITY FOR  $\psi > 1$

Operation	FDE		FD-DFE		IFIC-FD-DFE	
	Complexity	Value	Complexity	Value	Complexity	Value
Channel Estimation	$MNL$	$1.31 \times 10^6$	$MNL$	$1.31 \times 10^6$	$MNL$	$1.31 \times 10^6$
TR processing	$\mathcal{O}(MN \log_2 N)$	$7.68 \times 10^4$	$\mathcal{O}(MN \log_2 N)$	$7.68 \times 10^4$	$\mathcal{O}(MN \log_2 N)$	$7.68 \times 10^4$
Filter Calculation & Filtering	$2N$	$2.05 \times 10^3$	$2N$	$2.05 \times 10^3$	$2N$	$2.05 \times 10^3$
FFT/IFFT	$\frac{3}{2}N \log_2 N$	$1.54 \times 10^4$	$\frac{3}{2}N \log_2 N$	$1.54 \times 10^4$	$\frac{3}{2}N \log_2 N$	$1.54 \times 10^4$
Total		$1.40 \times 10^6$		$1.40 \times 10^6$		$1.40 \times 10^6$

Operation	FDE		FD-DFE		IFIC-FD-DFE	
	Complexity	Value	Complexity	Value	Complexity	Value
Channel Estimation	$MNL$	$1.31 \times 10^6$	$MNL$	$1.31 \times 10^6$	$\Omega MNL$	$3.59 \times 10^6$
TR processing	$\mathcal{O}(MN \log_2 N)$	$7.68 \times 10^4$	$\mathcal{O}(MN \log_2 N)$	$7.68 \times 10^4$	$\mathcal{O}((\Omega - 1)MNL)$	$2.45 \times 10^6$
Filter Calculation & Filtering	$2N$	$2.05 \times 10^3$	$4N$	$4.10 \times 10^3$	$2N(L + 1) + \frac{N}{2} \log_2 N$	$5.31 \times 10^5$
FFT/IFFT	$\frac{3}{2}N \log_2 N$	$1.54 \times 10^4$	$2N \log_2 N$	$2.05 \times 10^4$	$2N \log_2 N$	$2.05 \times 10^4$
Total		$1.40 \times 10^6$		$1.41 \times 10^6$		$6.59 \times 10^6$

The computational cost is counted for each block in one iteration, with the parameters of  $M = 5$ ,  $N = 1024$ ,  $L = 256$ , and  $\Omega = 2.74$ .

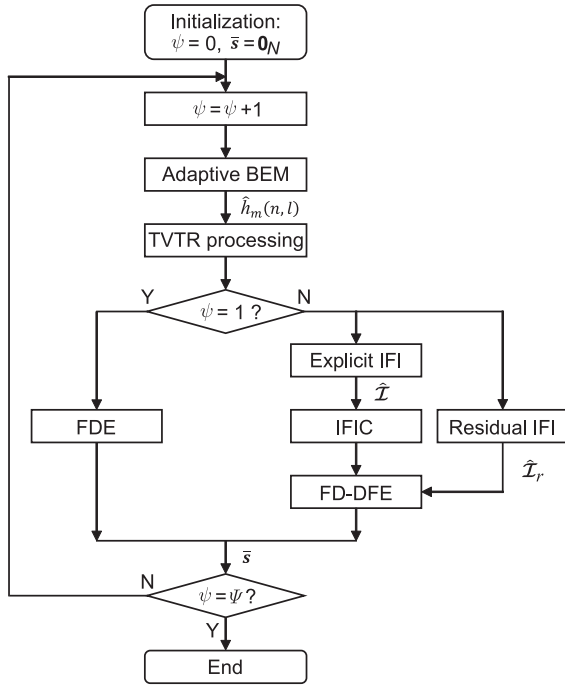


Fig. 3. Iterative processing for an individual block.

TR processing to obtain a single composite signal for equalization. In filter calculation and filtering operations, the complexity of the FD-DFE schemes is double that of FDE due to an additional feedback filter. The complexity of IFIC-FD-DFE is higher than those of other schemes because of the IFI calculation in (15a). For the FFT/IFFT transforms, three schemes have comparable complexity. Here, the example parameters in Section IV are used to calculate the detailed complexity. Note that

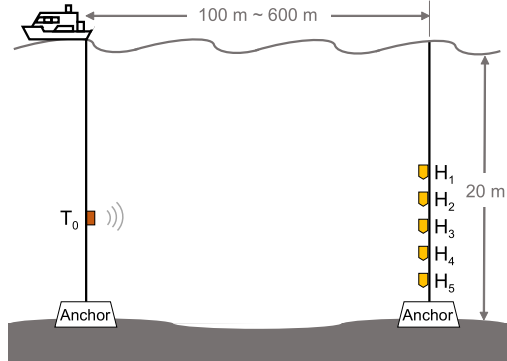


Fig. 4. Experimental setup at the Gulf of Mexico. The acoustic carrier frequency was 160 kHz.

the basis number  $\Omega$  is the average value. The FD-DFE scheme has almost the same complexity as the FDE receiver. The complexity of the IFIC-FD-DFE receiver is about five times those of the FDE and FD-DFE schemes.

#### IV. EXPERIMENTAL RESULTS

In this section, we present the results from the experiment at the Gulf of Mexico in August 2017. We compare the performance of three receivers: FDE, FD-DFE, and IFIC-FD-DFE. The IFI cancelation performance of the receivers is examined.

##### A. Experiment Description

The experiment was conducted at the Gulf of Mexico on August 21, 2017. The experiment site was about 17 nautical miles off the Alabama coast. The deployment setting is illustrated in Fig. 4. The water depth was 20 m. A 160-kHz transducer  $T_0$  was submerged at a depth of 15 m,

TABLE II  
TRANSCEIVER PARAMETERS

Parameters	Description	Values
$f_c$	Carrier frequency	160 kHz
$R_s$	Symbol rate	32 kHz
$B$	Bandwidth	40 kHz
$T_{pk}$	Packet duration	6.0 s
$N_{pk}$	Number of packets at each range	3 or 2 <sup>†</sup>
$M$	Number of receiving elements	5
$K$	Fractional sampling rate	4
$T$	Block duration	32 ms
$\beta$	Block overlapping rate	30%
$\Psi$	Iterations	4
$P$	Sparsity level in CoSaMP	20
$b_{lag}$	Block lag	13

<sup>†</sup>3 for 100-m range and 2 for other ranges.

hung from the Research Vessel (R/V) *Wilson*. A five-element broadband receiver array was deployed from the water depth of 10–18 m, with an element spacing of 2.0 m, on a mooring line. The R/V *Wilson* was anchored at four different ranges, i.e., 100, 200, 400, and 600 m, away from the moored receiver. During the acoustic transmissions, both the transmitter and the receiver array were stationary.

The QPSK signal at the center frequency of 160 kHz is of interest in the analysis. The signal was transmitted over a 40-kHz bandwidth at a symbol rate of 32 kHz. A rate-2/3 quasi-cyclic low-density parity-check (QC-LDPC) code with a  $519 \times 1557$  parity check matrix was used. At each range, either two or three communication packets were transmitted. The packet duration was 6.0 s. The transceiver parameters are listed in Table II.

### B. Receiver Implementation

The received signals were transformed to the baseband with the fractional sampling rate of  $K = 4$ . Resampling was then performed to suppress the dominant Doppler, which was no more than 25 Hz. After preprocessing, the data were partitioned into 32-ms blocks with the overlapping rate of  $\beta = 30\%$ . Doppler tracking and correction method in [31] was used to address the instantaneous Doppler. Considering the trade-off between the performance and complexity, we chose iterations  $\Psi = 4$  in demodulation. In the adaptive BEM estimator, the channel sparsity level, which is defined as the number of nonzero paths, was set as  $P = 20$ . First 13 blocks were used to estimate the initial correlation coefficients of channels.

Three types of receivers, FDE, FD-DFE, and IFIC-FD-DFE, have been studied for comparison using the at-sea measurements. All the receivers were implemented in the working mode, where only the training blocks were made known to the receiver. IFI cancellation gain, output SNR, uncoded BER, and coded BER were used as the performance metrics.

### C. Channel Characteristics

The estimated channel impulse responses at 100- and 600-m communication ranges are shown in Fig. 5. The acoustic arrivals are marked at the top of Fig. 5(a) and (c). The impulse response at the 600-m range had a smaller delay spread. That was a consequence of smaller grazing angles of acoustic arrivals for longer ranges. The smaller grazing angles also resulted in the micropaths spanning in a wider time spread with lower energy. That made the specular reflections dominate the arrivals.

TABLE III  
AVERAGE VALUES OF  $\Omega$  AT FIVE DEPTHS FOR FOUR COMMUNICATION RANGES

Hydrophone	Range (m)				Average
	100	200	400	600	
H <sub>1</sub>	3.0	3.0	3.0	2.8	2.95
H <sub>2</sub>	3.0	2.9	1.8	2.3	2.50
H <sub>3</sub>	3.0	2.6	3.0	2.5	2.78
H <sub>4</sub>	2.6	2.7	3.0	2.3	2.65
H <sub>5</sub>	2.8	3.0	3.0	2.4	2.80
Average	2.88	2.84	2.76	2.46	2.74

For the  $q$ -functions, their spreads were smaller than those of the impulse responses, as shown in Fig. 5(b) and (d).

The channel fluctuation rate varied at different communication ranges. The channel correlation coefficients for four ranges are shown in Fig. 6. As shown in Fig. 6(a), the coherence times for 100–400 m were about 20 ms. The channels for these communication ranges were fast time-varying channels. The coherence time for the 600-m range was the largest, which resulted from the stable direct path and specular-reflected multipaths. In comparison, the  $q$ -functions did not vary fast. They were segmented into two parts, “peaks” and “sidelobes.” The “peak” segment contained the central 0 ms of a  $q$ -function. The rest was treated as the “sidelobe” segment. The correlation coefficients for the “peak” and “sidelobe” segments of  $q$ -functions are shown in Fig. 6(b). The “peak” segment varied much slower than the “sidelobe” segment, whose coherence times were a bit higher than those of impulse responses in Fig. 6(a). Therefore, the slow time variance of  $q$ -function resulted from the “peak” arrival.

The value of  $\Omega$  also reveals the channel fluctuation rate indirectly, as it is calculated according to the channel Doppler spread or coherence time. Table III lists the values of  $\Omega$  at all measuring ranges and depths. They have been averaged across the blocks. In most cases,  $\Omega = 3$  was sufficient to characterize the channel variation. Along the range direction, the average  $\Omega$  became smaller with the longer ranges, indicating that the channel variation was getting slower. That was consistent with the previous analysis. Along the depth direction, the top  $\Omega$  value was larger than the others. That indicates a faster time-varying channel for the hydrophone close to the sea surface.

### D. Performance

We first examined the IFI and its cancelation performance in different receiver settings at 200-m communication range. As the IFI is closely related to the block duration, Fig. 7 shows the IFIs for two cases,  $T = 32$  ms and  $T = 48$  ms. The IFIs were calculated with (6) in the training mode. They both showed strong frequency dependence, with the lowest value at  $-1$  kHz. In the case where  $T = 32$  ms [see Fig. 7(a)], the average IFI was 6.9 dB before cancelation. The longer block introduced a larger IFI, as shown in Fig. 7(b), where  $T = 48$  ms. That was resulted from the larger time-varying component  $Q_v$  [see (6)].

With IFI cancelation, the IFI across the frequency band was well suppressed. For  $T = 32$  ms and  $T = 48$  ms, the average IFI reductions were, 5.7 and 6.9 dB, respectively, in the IFIC-FD-DFE receiver, as shown in Fig. 7(a) and (b). The residual IFI for  $T = 48$  ms was higher than that for  $T = 32$  ms.

We then evaluated the BER performance for the receivers with and without IFI cancelation in the same packet at 200-m range. Fig. 8 shows the BERs for the cases of  $T = 32$  ms and  $T = 48$  ms. In the case of  $T = 32$  ms [see Fig. 8(a)], the average BERs were, 4.3% and 3.3%, respectively, for the IFI-ignorant FDE and FD-DFE receivers.

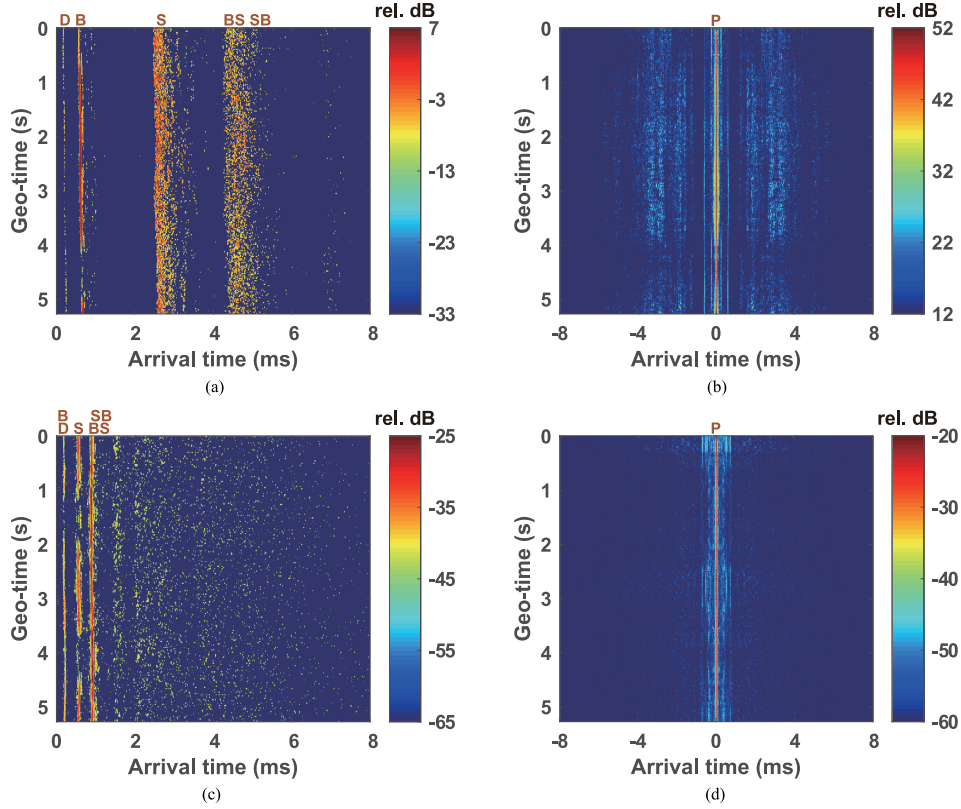


Fig. 5. Channel estimates between  $T_0$  and  $H_3$ . The acoustic arrivals are marked as D (direct arrival), B (bottom scattered arrival), S (surface scattered arrival), BS (bottom-surface scattered arrival), SB (surface-bottom scattered arrival), and P (peak arrival). (a) Impulse response at 100 m. (b)  $q$ -function at 100 m. (c) Impulse response at 600 m. (d)  $q$ -function at 600 m.

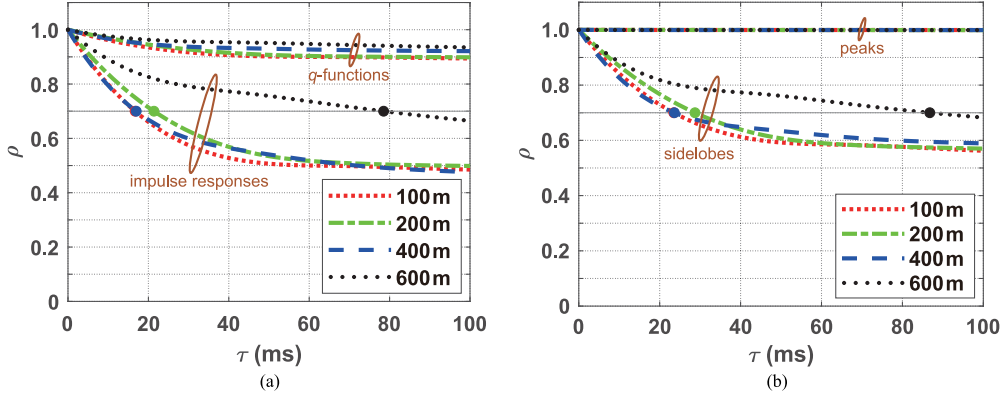


Fig. 6. Channel correlation coefficients in the 2017 Gulf experiment. (a) Correlation coefficients for impulse responses and  $q$ -functions. The coherence times of impulse responses were, 16.7, 21.4, 17.0, and 78.5 ms, respectively, for the four communication ranges. (b) Correlation coefficients for the “peak” and “sidelobe” segments of  $q$ -functions. The coherence times of the “sidelobe” segment were, 23.5, 28.7, 23.6, and 86.8 ms, respectively, for the four ranges.

For  $T = 48$  ms, the larger IFI level deteriorated the BERs, which were 5.6% and 4.5% for the FDE and FD-DDE receivers, as shown in Fig. 8(b).

In the IFIC-FD-DDE receiver, the BERs were reduced because of the IFI cancellation. For  $T = 32$  ms and  $T = 48$  ms, the average uncoded BERs were, 40% and 35%, respectively, lower in the IFIC-FD-DDE receiver than those in FD-DDE receivers, as shown in Fig. 8(a) and (b). The corresponding output SNR improvements were 1.4 and 1.1 dB, respectively. Due to the higher residual IFI, the BER performance for  $T = 48$  ms was worse than that for  $T = 32$  ms.

A shorter block introduces smaller IFI, but may lead to larger IFI estimation errors due to unreliable channel estimates. The performance of a shorter block duration (i.e.,  $T = 24$  ms) is shown in Table IV. In comparison with the receiver using  $T = 32$  ms, the one using  $T = 24$  ms suffered performance degradation caused by larger channel estimation errors.

To examine the impact of the iterative processing in the IFIC-FD-DDE receiver, we measured its output SNRs and uncoded BERs with different iterations. As shown in Fig. 9, the performance was improved with the increase of iterations. In the first iteration, most packets failed,

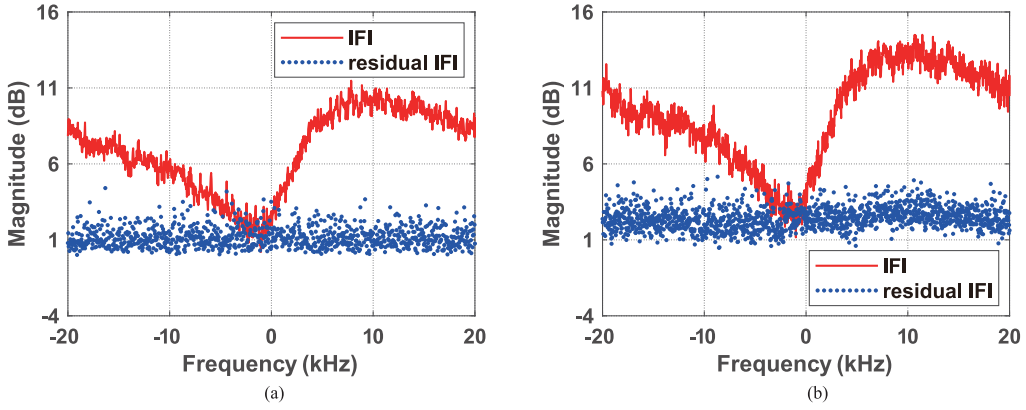


Fig. 7. IFIs and residual IFIs in one packet at the 200-m range. (a) IFIs for  $T = 32$  ms. The average IFI and residual IFI were 6.9 and 1.2 dB, respectively. (b) IFIs for  $T = 48$  ms. The average IFI and residual IFI were 9.3 and 2.4 dB, respectively.

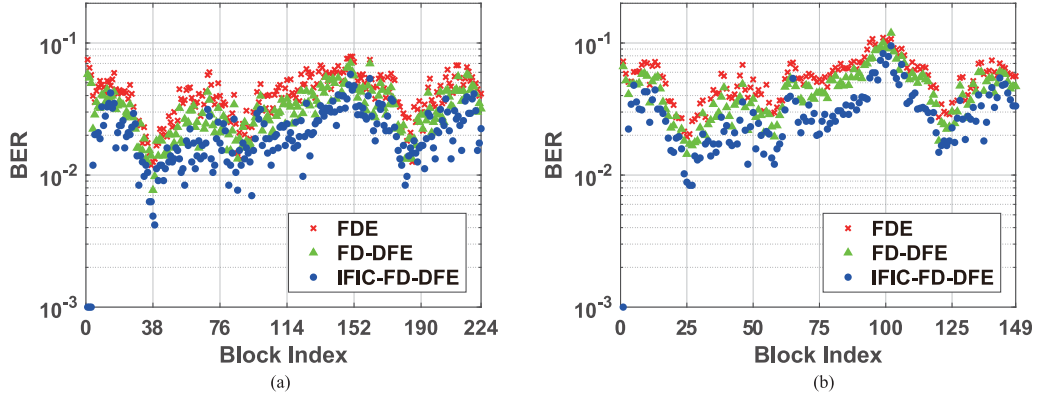


Fig. 8. Block BERs in one packet at the 200-m range for FDE, FD-DFE, and IFIC-FD-DFE receivers. Note that the block BERs of  $10^{-3}$  refer to 0. (a) Block BERs for  $T = 32$  ms. The average BERs for three receivers were 4.3%, 3.3%, and 2.0%, respectively. (b) Block BERs for  $T = 48$  ms. The average BERs for three receivers were 5.6%, 4.5%, and 2.9%.

TABLE IV  
PERFORMANCE COMPARISON BETWEEN IFIC-FD-DFE RECEIVERS WITH  
 $T = 24$  ms AND  $T = 32$  ms AT FOUR COMMUNICATION RANGES

Range (m)	Output SNR (dB)		Uncoded BER	
	$T = 24$ ms	$T = 32$ ms	$T = 24$ ms	$T = 32$ ms
100	10.1	9.8	0.8%	0.6%
200	7.8	7.8	2.6%	2.0%
400	5.9	6.1	6.0%	4.6%
600	5.9	6.0	5.9%	4.6%

as the IFI was ignored, and the equalizer coefficients were calculated from the outdated  $q$ -function in the previous block. In comparison, the average output SNR was improved by 6.2 dB at iteration four, and the average uncoded BER decreased by 85%. More iterations beyond four led to negligible performance improvements.

We compared the IFIC-FD-DFE receiver with the time-domain DFE receiver in [1]. In the time-domain DFE receiver, we applied the soft-symbol-based iterative scheme for a fair comparison. To achieve the best performance, we optimized the receiver parameters, such as the proportional and integral tracking constants. Most of the packets failed with the time-domain DFE, whereas IFIC-FD-DFE successfully decoded all packets. Fig. 10 shows the scatter plots with these two

receivers in one successful packet at the 100-m range. It shows that our receiver performed almost 4 dB better than the time-domain DFE for this packet. In addition, the time-domain DFE requires periodic training symbols to alleviate the error propagation. In this case, 25% training symbols were used. For our IFIC-FD-DFE, the training symbol length was 5.5%, which was much shorter.

Performance comparisons among the FDE, FD-DFE, and IFIC-FD-DFE receivers are listed in Table V, where the output SNRs, uncoded BERs, and coded BERs are shown for individual ranges. At 100-, 200-, and 600-m communication ranges, no packet failed for all three receivers. At 400-m range, the FDE and FD-DFE receivers both failed at Packet 1 while IFIC-FD-DFE succeeded. All three receivers succeeded at Packet 2. Only Packet 2 was used for a fair comparison. On average, the IFIC-FD-DFE receiver outperformed the FDE and FD-DFE ones by 1.9 and 1.2 dB, respectively. The uncoded BER was 40% less than that of the FDE receiver, and was 30% less than that of the FD-DFE receiver. At 600-m range, the performance gains for the new receiver over the other two receivers were less significant. That was a consequence of lower level of IFI under slower channel variations.

In the TVTR-FD-DFE receiver, both the TVTR processing and explicit IFIC modules suppressed the IFI. As shown in Table V, the TVTR processing led to a 1.0-dB gain for the FD-DFE in terms of average output SNR. The gain was attributed to the focused  $q$ -functions,

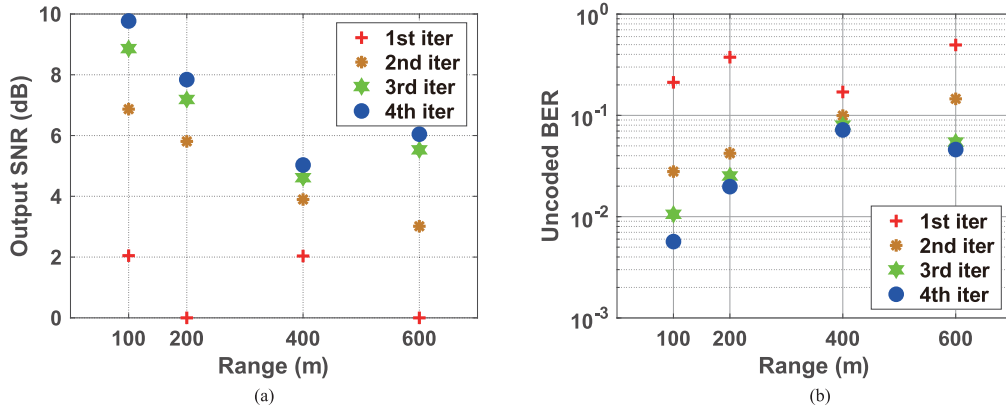


Fig. 9. Performance improvements of iterations in the IFIC-FD-DFE receiver. (a) Output SNRs. (b) Uncoded BERs.

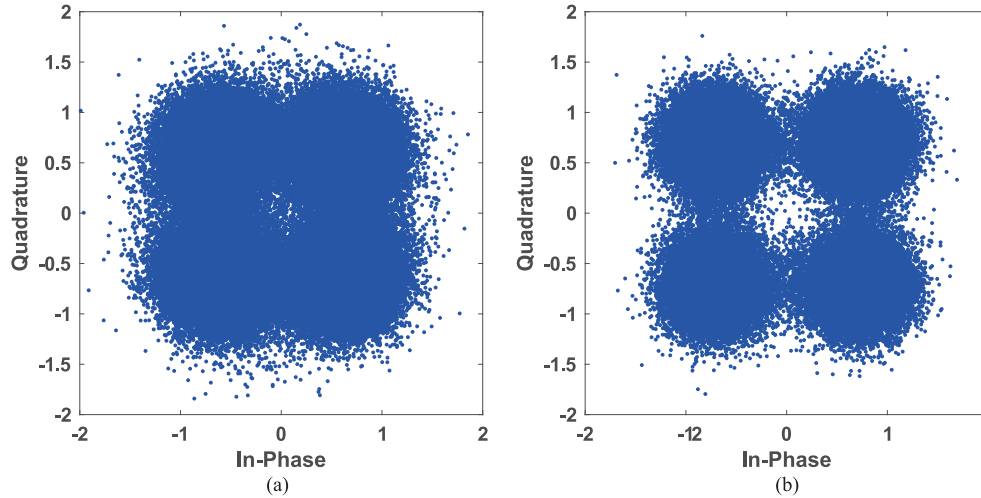


Fig. 10. Scatter plots in one packet at the 100-m range. (a) Scatter plot of time-domain DFE. The output SNR was 6.5 dB, and the uncoded BER was 3.3%. (b) Scatter plot of IFIC-FD-DFE. The output SNR was 10.4 dB, and the uncoded BER was 0.3%.

TABLE V  
PERFORMANCE COMPARISON AMONG THE FDE, FD-DFE, AND IFIC-FD-DFE RECEIVERS AT FOUR COMMUNICATION RANGES

Range (m)	Output SNR (dB)				Uncoded BER				Coded BER			
	FDE	FD-DFE	TVTR-FD-DFE	IFIC-FD-DFE	FDE	FD-DFE	TVTR-FD-DFE	IFIC-FD-DFE	FDE	FD-DFE	TVTR-FD-DFE	IFIC-FD-DFE
100	7.2	8.1	9.0	9.8	1.7%	1.2%	0.7%	0.6%	0.01%	0	0	0
200	5.4	6.4	7.6	7.8	4.1%	3.0%	1.9%	2.0%	0.20%	0.02%	0	0
400	4.5	4.9	6.1	6.1	6.8%	6.2%	4.5%	4.6%	3.83%	3.28%	1.30%	1.37%
600	4.9	5.5	6.0	6.0	5.5%	4.8%	4.5%	4.6%	1.42%	0.78%	0.34%	0.30%

whose peak values were 0.8 dB higher than those in the regular TR processing. That made the IFI component relatively smaller in TVTR-FD-DFE according to (5). If the explicit IFIC was used, an additional 0.8-dB gain was achieved at the 100-m range. At the 200-m range, the gain was 0.2 dB. At longer ranges, the performance improvement was minimum. The reason was that the main IFI was suppressed by the TVTR processing.

Receiver performance metrics with QC-LDPC codes are also listed in Table V. The IFIC-FD-DFE exhibited improvements over the other two receivers. At the short ranges of 100 and 200 m, the BERs were close

to zero for the FD-DFE-based receivers. At the range of 400 m, the BER reductions of TVTR-FD-DFE or IFIC-FD-DFE were, respectively, 65% and 60% in comparison with those of the other two receivers. At the range of 600 m, those BER reductions were 80% and 60%.

## V. CONCLUSION

To explicitly address the IFI induced by the fast time-varying UWA channel, we proposed a blockwise FD-DFE scheme to demodulate single-carrier transmissions. The soft iterative receiver, referred to as

IFIC-FD-DFE, iterates the impulse responses, explicit IFI estimates, and residual IFI calculation based on the soft symbol estimates. The effectiveness of the IFIC-FD-DFE scheme was demonstrated using the measurements collected from the Gulf of Mexico in August 2017. Three types of receivers, FDE, FD-DFE, and IFIC-FD-DFE, were tested with the field measurements, which contained communication packets from four communication ranges at 100, 200, 400, and 600 m. Two or three communication packets were transmitted at each range.

The IFIC-FD-DFE receiver uses two main procedures, the TVTR processing and explicit IFIC, to address the IFI. The IFI was suppressed by an average 5.5 dB among four communication ranges, leading to a 1.2-dB improvement over the receiver without IFI cancellation. We also showed that the shorter blocks led to larger IFI estimation errors, whereas the longer blocks led to higher residual IFI. With the soft iterative operation, the IFI cancellation performance was enhanced, leading to a 6.2-dB gain in the output SNR. Overall, the proposed receiver outperformed the conventional FDE, FD-DFE, and time-domain DFE receivers. For the FDE and FD-DFE receivers, one packet failed at the 400-m communication range. For the time-domain DFE receiver, most of the packets failed. In comparison, all packets were successfully decoded using the IFIC-FD-DFE receiver. The transmissions of a coded data rate of 42.7 kb/s were achieved at four ranges, from 100 to 600 m.

#### ACKNOWLEDGMENT

The authors would like to express gratitude to the marine support from the Dauphin Island Sea Laboratory (DISL), Dauphin Island, AL, USA. Gr. Lockridge from the DISL provided tremendous help in mooring preparation and during at-sea operations. The authors would like to thank all participants of the 2017 Gulf Acoustic Experiment. The content, statements, findings, opinions, conclusion, and recommendations are those of the author(s) and do not necessarily reflect the views of the State of Texas or the Treasury.

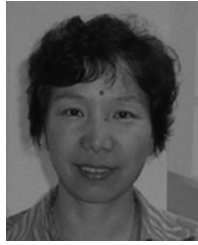
#### REFERENCES

- [1] M. Stojanovic, "Acoustic (underwater) communications," in *Encyclopedia of Telecommunications*, 1st ed., J. G. Proakis, Ed. New York, NY, USA: Wiley, 2003, vol. 1, pp. 36–47.
- [2] Y. R. Zheng, C. Xiao, T. Yang, and W.-B. Yang, "Frequency-domain channel estimation and equalization for shallow-water acoustic communications," *Phys. Commun.*, vol. 3, no. 1, pp. 48–63, 2010.
- [3] L. Wang, J. Tao, C. Xiao, and T. Yang, "Low-complexity turbo detection for single-carrier low-density parity-check-coded multiple-input multiple-output underwater acoustic communications," *Wireless Commun. Mobile Comput.*, vol. 13, no. 4, pp. 439–450, 2013.
- [4] M. Xia, D. Rouseff, J. A. Ritcey, X. Zou, C. Polprasert, and W. Xu, "Underwater acoustic communication in a highly refractive environment using SC-FDE," *IEEE J. Ocean. Eng.*, vol. 39, no. 3, pp. 491–499, Jul. 2014.
- [5] J. Huang, S. Zhou, J. Huang, C. R. Berger, and P. Willett, "Progressive inter-carrier interference equalization for OFDM transmission over time-varying underwater acoustic channels," *IEEE J. Sel. Topics Signal Process.*, vol. 5, no. 8, pp. 1524–1536, Dec. 2011.
- [6] N. Benvenuto, R. Dinis, D. Falconer, and S. Tomasin, "Single carrier modulation with nonlinear frequency domain equalization: An idea whose time has come—Again," *Proc. IEEE*, vol. 98, no. 1, pp. 69–96, Jan. 2010.
- [7] J. C. Preisig, A. C. Singer, and G. W. Wornell, "Reduced bandwidth frequency domain equalization for underwater acoustic communications," in *Proc. IEEE Sens. Array Multichannel Signal Process. Workshop*, 2010, pp. 93–96.
- [8] C. He, S. Huo, H. Wang, Q. Zhang, and J. Huang, "Single carrier with multi-channel time-frequency domain equalization for underwater acoustic communications," in *Proc. IEEE Int. Conf. Acoust. Speech Signal Process.*, 2015, pp. 3009–3013.
- [9] C. He, R. Xi, H. Wang, L. Jing, W. Shi, and Q. Zhang, "Single carrier with frequency domain equalization for synthetic aperture underwater acoustic communications," *Sensors*, vol. 17, no. 7, 2017, Art. no. 1584.
- [10] Z. Chen, J. Wang, and Y. R. Zheng, "Frequency-domain turbo equalization with iterative channel estimation for MIMO underwater acoustic communications," *IEEE J. Ocean. Eng.*, vol. 42, no. 3, pp. 711–721, Jul. 2017.
- [11] N. Benvenuto and S. Tomasin, "Iterative design and detection of a DFE in the frequency domain," *IEEE Trans. Commun.*, vol. 53, no. 11, pp. 1867–1875, Nov. 2005.
- [12] P. Montezuma, F. Silva, and R. Dinis, "Block transmission techniques," in *Frequency-Domain Receiver Design for Doubly Selective Channels*. Boca Raton, FL, USA: CRC Press, 2017, ch. 3.
- [13] N. Souto, R. Dinis, and J. C. Silva, "Reliability of an IB-DFE in the presence of channel estimation errors," in *Proc. IEEE 77th Veh. Technol. Conf.*, 2013, pp. 1–5.
- [14] W. Duan, Y. R. Zheng, D. Sun, and Y. Zhang, "Block iterative FDE for MIMO underwater acoustic communications," in *Proc. IEEE/OES China Ocean Acoust. Symp.*, 2016, pp. 1–4.
- [15] C. He, S. Huo, Q. Zhang, H. Wang, and J. Huang, "Multi-channel iterative FDE for single carrier block transmission over underwater acoustic channels," *China Commun.*, vol. 12, no. 8, pp. 55–61, 2015.
- [16] Y. R. Zheng, J. Wu, and C. Xiao, "Turbo equalization for single-carrier underwater acoustic communications," *IEEE Commun. Mag.*, vol. 53, no. 11, pp. 79–87, Nov. 2015.
- [17] J. Tao, Y. R. Zheng, C. Xiao, and T. Yang, "Robust MIMO underwater acoustic communications using turbo block decision-feedback equalization," *IEEE J. Ocean. Eng.*, vol. 35, no. 4, pp. 948–960, Oct. 2010.
- [18] J. Zhang and Y. R. Zheng, "Frequency-domain turbo equalization with soft successive interference cancellation for single carrier MIMO underwater acoustic communications," *IEEE Trans. Wireless Commun.*, vol. 10, no. 9, pp. 2872–2882, Sep. 2011.
- [19] K. Tu, D. Fertonani, T. M. Duman, M. Stojanovic, J. G. Proakis, and P. Hurksy, "Mitigation of intercarrier interference for OFDM over time-varying underwater acoustic channels," *IEEE J. Ocean. Eng.*, vol. 36, no. 2, pp. 156–171, Apr. 2011.
- [20] H. Yu, A. Song, M. Badiey, F. Chen, and F. Ji, "Iterative estimation of doubly selective underwater acoustic channel using basis expansion models," *Ad Hoc Netw.*, vol. 34, pp. 52–61, 2015.
- [21] Z. Xie, X. Chen, and X. Liu, "A virtual pilot-assisted channel estimation algorithm for MIMO-SCFDE systems over fast time-varying multipath channels," *IEEE Trans. Veh. Technol.*, vol. 67, no. 6, Jun. 2018, Art. no. 4901.
- [22] L.-N. Tran, E.-K. Hong, and H. Liu, "A frequency domain equalization algorithm for fast time-varying fading channels," *J. Commun. Netw.*, vol. 11, no. 5, pp. 474–480, 2009.
- [23] Z. Xie, X. Chen, and C. Li, "A novel joint channel estimation and equalization algorithm for MIMO-SCFDE systems over doubly selective channels," *Digit. Signal Process.*, vol. 75, pp. 202–209, 2018.
- [24] L. Dong, "Receiver design for single-carrier block transmission over doubly selective channels," *Wireless Pers. Commun.*, vol. 77, no. 3, pp. 1833–1845, 2014.
- [25] X. Tu, A. Song, and X. Xu, "Prefix-free frequency domain equalization for underwater acoustic single carrier transmissions," *IEEE Access*, vol. 6, pp. 2578–2588, 2018.
- [26] W.-J. Zeng and X. Jiang, "Time reversal communication over doubly spread channels," *J. Acoust. Soc. Amer.*, vol. 132, no. 5, pp. 3200–3212, 2012.
- [27] D. Needell and J. A. Tropp, "CoSaMP: Iterative signal recovery from incomplete and inaccurate samples," *Appl. Comput. Harmon. Anal.*, vol. 26, no. 3, pp. 301–321, 2009.
- [28] F. Qu and L. Yang, "Basis expansion model for underwater acoustic channels?" in *Proc. IEEE OCEANS Conf.*, 2008, pp. 1–7.
- [29] R. Steele and L. Hanzo, "Mobile radio channels," in *Mobile Radio Communications: Second and Third Generation Cellular and WATM Systems*, 2nd ed. Chichester, U.K.: Wiley–IEEE Press, 1999, ch. 2.
- [30] A. Gusmao, P. Torres, R. Dinis, and N. Esteves, "A turbo FDE technique for reduced-CP SC-based block transmission systems," *IEEE Trans. Commun.*, vol. 55, no. 1, pp. 16–20, Jan. 2007.
- [31] A. Song, M. Badiey, V. K. McDonald, and T. C. Yang, "Time reversal receivers for high data rate acoustic multiple-input–multiple-output communication," *IEEE J. Ocean. Eng.*, vol. 36, no. 4, pp. 525–538, Oct. 2011.



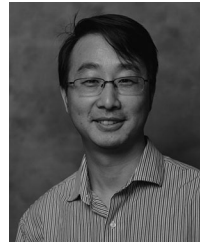
**Xingbin Tu** received the B.S. degree in marine physics from the College of Ocean and Earth Science, Xiamen University, Xiamen, China, in 2012. He is currently working toward the Ph.D. degree in marine physics with Xiamen University.

In 2014, he enrolled from the master's program into the doctoral program. From 2016 to 2018, he was a Visiting Scholar with the Department of Electrical and Computer Engineering, University of Alabama, Tuscaloosa, AL, USA. His research interests include underwater acoustic communications and signal processing.



**Xiaomei Xu** received the M.S. degree in underwater acoustic telemetry and the Ph.D. degree in underwater communications from Xiamen University, Xiamen, China, in 1988 and 2002, respectively.

In 1994 and 1995, she was a Visiting Scholar with the Department of Electrical and Computer Engineering, Oregon State University, Corvallis, OR, USA. She is currently a Professor with the College of Ocean and Earth Science, Xiamen University. Her research interests include underwater communication, underwater acoustic telemetry, and underwater acoustic networks.



**Aijun Song** (Member, IEEE) received the Ph.D. degree in electrical engineering from the University of Delaware, Newark, DE, USA, in 2005.

He is currently an Assistant Professor with the Department of Electrical and Computer Engineering, University of Alabama, Tuscaloosa, AL, USA. From 2005 to 2008, he was a Postdoctoral Research Associate at the College of Earth, Ocean and Environment, University of Delaware. During this period, he was also an Office of Naval Research (ONR) Postdoctoral Fellow, supported by the Special Research Award in

the ONR Ocean Acoustics Program. He was an Assistant Research Professor with the University of Delaware from 2008 to 2014 and an Associate Research Professor from 2014 to 2015. Since 2015, he has been an Assistant Professor with the Department of Electrical and Computer Engineering, University of Alabama. His current research interests include digital communications and signal processing techniques for radio-frequency and underwater acoustic channels, ocean acoustics, sensor networks, and ocean monitoring and exploration. His general interests include underwater acoustic signal propagation, digital communication theory, and advanced signal processing in mobile radio frequency, and underwater acoustic environments.

Dr. Song was the General Co-Chair of 2018 March NSF Workshop on Underwater Wireless Communications and Networking and 2018 November NSF Workshop on Underwater Wireless Infrastructure. He was the General Co-Chair of the 14th International Conference on Underwater Networks & Systems (WUWNet'19).